HHS Public Access

Author manuscript

Gene Ther. Author manuscript; available in PMC 2013 November 01.

Published in final edited form as:

Gene Ther. 2013 May ; 20(5): 567–574. doi:10.1038/gt.2012.71.

Viral Dose, Radioiodine Uptake, and Delayed Efflux in Adenovirus Mediated NIS Radiovirotherapy Correlates with Treatment Efficacy

Miguel A. Trujillo[1], **Michael J. Oneal**[2], **Samantha McDonough**[1], and **John C. Morris**[1,3]

[1]Division of Endocrinology, Diabetes, Metabolism, Nutrition, Mayo Clinic, Rochester, MN

[2]Department of Molecular Medicine, Mayo Clinic, Rochester, MN Rochester, Minnesota 55905

Abstract

We have constructed a prostate tumor specific conditionally replicating adenovirus (CRAd), named Ad5PB_RSV-NIS that expresses the human sodium iodine symporter gene (hNIS). LNCaP tumors were established in nude mice and infected with this CRAd to study tumor viral spread, NIS expression, and efficacy. Using quantitative polymerase chain reaction (QPCR) we found a linear correlation between the viral dose and viral genome copy numbers recovered after tumor infection. Confocal microscopy showed a linear correlation between adenovirus density and NIS expression. Radioiodine uptake vs. virus dose-response curves revealed that the dose response curve was not linear and displayed a lower threshold of detection at 10^7 vp and an upper plateau of uptake at 10^{11} vp. The outcome of radiovirotherapy was highly dependent upon viral dose. At 10^{10} vp no significant differences were observed between virotherapy alone or radiovirotherapy. However, when radioiodine therapy was combined with virotherapy at a dose of 10^{11} vp, significant improvement in survival was observed, indicating a relationship between viral dose-response uptake and the efficacy of radiovirotherapy. The reasons behind the differences in radioiodine therapy efficacy can be ascribed to more efficient viral tumor spread and a decrease in the rate of radioisotope efflux. Our results have important implications regarding the desirables and undesirable characteristics of vectors for clinical translation of virus-mediated NIS transfer therapy

Keywords

prostate cancer; probasin; adenovirus; sodium iodide symporter; virotherapy; gene therapy

[3]Address Correspondence to: John C. Morris[1], Division of Endocrinology, Diabetes, Metabolism, Nutrition, Mayo Clinic, Rochester 200 First Street SW Rochester, MN 55905, Telephone: 284-3844/284-9655, morris.john@mayo.edu.

AUTHOR DISCLOSURE STATEMENT

No competing financial interests exist

Introduction

Prostate cancer is the second most frequently diagnosed cancer and sixth most frequent cause of cancer death in men worldwide [1]. To date, no uniformly curative therapy for metastatic prostate cancer has been developed. In some malignancies, for which existing treatment regimens are not completely effective, suicide gene therapy and virotherapy strategies targeting the tumor-associated genetic alterations represent rational directions for the development of novel therapeutics [2–4].

The sodium iodide symporter (NIS) is a transmembrane glycoprotein that mediates uptake of iodide into cells, especially thyroid follicular cells [5, 6]. The presence of NIS on the basolateral membrane of thyroid cells has been exploited for many years for diagnostic imaging purposes as well as for ablative therapy of benign thyroid disease and differentiated thyroid cancer using radioactive iodide (^{131}I). This non-invasive therapy has proven to be a safe and effective treatment for thyroid cancer, even in advanced, metastatic disease [7, 8]. In order to extend the use of NIS-mediated radioiodine therapy to other types of cancer, we have successfully transferred and expressed the sodium-iodide symporter (NIS) gene in prostate [9], colon [10], and breast cancer cells [11], both *in vivo* and *in vitro*, using adenoviral vectors. Our experience with adenovirus-mediated NIS transfer and radioiodine therapy was confirmed in large animal model and has culminated in the opening of a phase I trial for prostate cancer that is currently accruing patients [12, 13].

In addition to its therapeutic potential, NIS transfer allows for non-invasive imaging. NIS mediated imaging has been used to: confirm viral infection and NIS gene expression and function [14], quantitate intratumoral radioisotope uptake *in vivo* [15], monitor ectopic expression of the NIS gene *in vivo* in biodistribution studies [16], and to determine optimal therapeutic ^{131}I delivery timing [9]. Groot-Wassink *et al*. correlated NIS mediated radioiodine uptake to viral injected doses and NIS mRNA expression by imaging [17]. Although a linear correlation between PET scanning and postmortem γ counts in healthy liver was found, the correlation between viral dose (and NIS mRNA) to radioiodine uptake was non-linear. Thus, the relationship between NIS-mediated radioiodine uptake and the viral dose injected in tumors is unclear. In addition, a clear relationship between radioiodine uptake and efficacy has not yet been established.

We have developed a prostate specific, conditionally replicating adenoviral vector that also harbors the NIS gene [9]. In this conditionally replicating adenovirus (CRAd) Ad5PB_RSV-NIS, the transcriptional control of the E1A gene is governed by a composite probasin promoter targeting prostate cells in order to reduce extratumoral toxicity by induction of tumor selective replication and cell lysis. NIS expression allows for non- invasive imaging and reporting as well as the potential for radioiodine mediated therapy. This combination of virus mediated oncolysis and NIS mediated radioiodine therapy has been termed by Dingli et al, “Radiovirotherapy” [18].

In this report we have employed a xenograft model using LNCaP cells in nude mice which are transduced *in vivo* with the Ad5PB_RSV-NIS CRAd. Confocal microscopy and SPECT/CT NIS imaging were used to analyze tumor viral spread. We have also established

radioiodine uptake versus viral dose-response curves and have correlated our imaging studies to radiovirotherapy treatment efficacy. The results show that the outcome of radiovirotherapy is greatly dependent upon viral spread within the tumor. Moreover, we show that the radioiodine uptake vs. viral dose-response curve is complex, steep, and limited by a lower and an upper plateau of uptake. We also present evidence indicating that the upper imaging threshold further defines a minimal viral-dose for effective radiovirotherapy. We have found that radioiodine efflux and viral spread are major components in treatment outcome. We discuss how our results impact upon the clinical translation of virus-mediated NIS transfer therapy.

Results

Correlation between injected and viral dose delivered in intratumoral injection

In order to measure the number of viral genome copies that are actually present within the tumor after intratumoral injection, we performed QPCR assays of tumor samples after virus injection. LNCaP xenograft tumors established in nude mice were infected with a single dose of Ad5PB_RSV-NIS at 10^7, 10^9, or 10^{11} vp. Three days post-injection, animals were sacrificed and the tumors were tested for viral genome copy contents. Each tumor was assayed in triplicate. Figure 1 shows a linear correlation between the viral dose injected and the numbers of viral genome copies recovered. Thus, at a dose of 10^{11} vp, 1.88×10^7 genome copies/mg of tumor were recovered. Because the ratio of vp to pfu in our preparation is 100/1, this result indicated that approximately 1 in 50 pfu of injected virus was detectable in the tumor at day 3.

Correlation between viral presence and NIS expression

We delivered the Ad5PB_RSV-NIS CRAd intratumorally to four different mice at a dose of 10^{11} vp. On days three and ten, two mice were sacrificed and their tumors removed and frozen after immersion in OCT. Four μm slide sections obtained from the tumors were stained for Ad5 hexon (FITC) and NIS (Texas Red). Uninfected tumors were also process similarly and used as controls. At least twenty five photographs spanning the whole slides were taken from each tumor. No signal was detected in the control tumors (Figure 2A). Clear Ad5 foci can be seen on infected tumors both at day 3 (Figure 2B) and day 10 (Not Shown) indicating persistence of virus infection. The virus was spread throughout the tumor as it was found in 80 out of 82 (98%) of the images analyzed. NIS expression was restricted to areas of virus infection (Figures 2B). Both hexon and NIS signal were quantitated by counting the intensity of green and red pixels in each slide. The values obtained for days 3 and 10 were plotted against each other (Figures 2C and 2D). A linear correlation between green pixels (hexon) and red pixels (NIS) was found which was virtually identical between the two time points (r^2=0.73, slope=1.23). These data indicate that NIS expression was proportional to the virus load within the tumor and this correlation was independent of time.

Viral dose response measured by in vivo NIS imaging

Having determined that the correlations between viral dose injected and tumor virus load and between tumor virus load and NIS protein expression were both linear, we next studied how the level of NIS-mediated radioisotope uptake varied as a function of viral dose. When

LNCaP xenografted tumors reached approximately 200 mm^3, a single dose of Ad5PB_RSV-NIS at 10^7, 10^9, 10^{10} or 10^{11} vp was administered intratumorally. NIS mediated ^{99}Tc uptake was visualized and quantitated using micro SPECT-CT imaging. Figure 3A shows uptake of the radiotracer in the stomach and the thyroid due to native NIS expression as well as in the bladder as a result of tracer clearance in the urine [19]. Figure 3A also shows that virus mediated NIS expression resulted in tumor uptake of ^{99}Tc and that the strength of the signal increased with viral dose. To further ascertain the nature of NIS expression as a function of the viral dose, we quantified the levels of ^{99}Tc uptake as a function of the concentration of virus delivered into the tumor. At days 1, 2, and 3 post-injection, three mice per dose were analyzed. At each time point 0.5 μCi ^{99}Tc was administered i.p. and the uptake was visualized and quantified by micro SPECT-CT imaging. The results are shown in Figure 3B. For each dose, uptake remained fairly constant throughout the duration of the study except for the 10^{10} vp dose in which a small linear increase was detected. While at all doses tested we observed that NIS expression mediated ^{99}Tc uptake above that seen in the uninfected control, surprisingly the level of uptake varied very only slightly between the doses of 10^7 to 10^{10} vp then increased three fold at 10^{11} vp. The day three dose response curve was plotted and demonstrated a steep increase in radiotracer uptake between the doses of 10^9 and 10^{11} vp (Figure 4A).

Because we showed in Figure 1 a linear relationship between dose injected and the number of viral genome copies, we plotted the dose response curve as function of genome copies per mg of tumor. This curve was plotted and fitted for viral doses between 10^7 and 10^{11} vp. For the dose interval analyzed, the dose response curve could only be fitted by a very steep logistic function as shown in Figure 4B. This result indicated that measurable NIS-mediated uptake has a lower threshold of detection at approximately 10^7 vp and an upper plateau of uptake at 10^{11} vp.

Correlation between viral dose response and efficacy

We have shown previously with this vector that the combination of radiotherapy and cytolytic virotherapy was superior to virotherapy alone [9]. In light of the finding of a very steep virus dose-response with a lower threshold and an upper plateau, we wished to determine the effect of this phenomenon on the efficacy of radiovirotherapy. To address this question, LNCaP xenografts were established in seven groups of mice (average group size n=10±3). One group of mice was used as control (C), four groups received a single intratumoral dose of Ad5PB_RSV-NIS at 10^9, 10^{10} or 10^{11} vp each (virotherapy V), and the following four groups received each a single intratumoral injection of Ad5PB_RSV-NIS at the aforementioned vp doses and 4 days later a single intraperitoneal dose of 3 mCi ^{131}I. The survival of each group was determined using Kaplan-Meier curves (Figure 5). The survival times were subjected to a Cox proportional hazards survival regression model (Figure 5). Treatment of tumors with Ad5PB_RSV-NIS at a dose of 10^9 vp resulted in no significant difference compared to the untreated control cohort. A modest improvement in the outcome was observed when radioiodine was also administered, but this difference was not statistically significant when compared to the control group. A therapeutic effect was observed at a viral dose of 10^{10} vp. However, at this viral dose, radioiodine treatment did not improve efficacy of the treatment. Compared to 10^{10} vp plus or minus radioiodine, no

significant differences were observed at a dose of 10^{11} vp. However, when radioiodine therapy was combined with virotherapy at a dose of 10^{11} vp, a major improvement on the outcome of the treatment was observed (Figure 5). Thus, the observed radioiodine viral dose-response uptake (Figure 4) correlated with the efficacy of radiovirotherapy.

Pinhole imaging and radioisotope efflux

We hypothesized that the differences in radioiodine therapy efficacy observed between the doses of 10^{10} and 10^{11} vp may be due to improved viral spread and dispersion. As indicated above, using confocal microscopy, we observed that upon delivering a dose of 10^{11} vp, the virus was better dispersed throughout the tumor. We examined this further using pinhole micro-SPECT/CT to compare in vivo virus distribution as reported by radionuclide uptake between a dose of 10^{10} and 10^{11} vp. This technique has been previously shown to accurately resolve viral intratumoral dispersion patterns [20].

LNCaP xenografts were established in the flanks of nude mice. When the xenografted tumors reached approximately 200 mm^3, a single dose of Ad5PB_RSV-NIS at 10^{10} or 10^{11} vp was administered intratumorally and NIS mediated ^{99}Tc uptake was visualized. Figure 6A shows that at 10^{10} vp discrete foci of virus infection were formed within the tumor leaving large areas of tissue where no detectable viral signal was detected. On the other hand, the pinhole imaging at 10^{11} vp indicated that the virus was evenly distributed throughout the tumor (Figure 6B). Thus, this data indicates that the difference in radiovirotherapy between the 10^{10} vp dose and the 10^{11} vp dose may reside in a better viral dispersion at higher viral doses.

In addition we determined the amount of remaining ^{99}mTc-pertechnetate in the tumor of mice injected intratumorally with 10^{10} or 10^{11} vp as a function of time (Figure 6C). When tumors were infected with Ad5PB_RSV-NIS at 10^{11} vp tracer efflux kinetics yielded a $t_{1/2}$ of 6.8 h while at 10^{10} vp the $t_{1/2}$ was 3.9 h. Moreover, comparison of the area under the curve between the two doses indicated that the amount of radioisotope retained was 3 times higher in tumors receiving 10^{11} vp compared to those receiving 10^{10} vp.

Discussion

We have reported the use of prostate targeted conditionally replicating adenoviruses expressing the NIS protein in *in vivo* mouse models of prostate cancer [9]. We have shown in this report that measurable NIS-mediated radioisotope uptake has a lower threshold of detection at 10^7 vp and an upper plateau of uptake at 10^{11} vp which correspond to 1.88×10^7 genome copies/mg of tumor, with a very steep viral dose-response curve. The observed radioiodine viral dose-response uptake correlates well with radiovirotherapy efficacy. Thus, we showed that radioiodine therapy is only effective when approximately 10^7 genome copies/mg of tumor were present within the tumor. At these higher doses, the virus was also dispersed more homogeneously within the tumor. NIS expression was linearly correlated to hexon expression with a Hexon:NIS ratio of ~1.2, indicating that almost all infected tumor cells expressed NIS.

As shown by the pinhole imaging studies, at an injected dose of 10^{11} vp, robust NIS expression covering the entire tumor was observed. In contrast, at lower viral doses effective NIS expression was limited to discrete foci within the tumors. It is likely that, at these low viral doses, tumor cell killing would be restricted to isolated regions within the tumor while at higher doses the killing would be extended to larger areas of the tumor. NIS can mediate robust bystander effects through ^{131}I decay β particle emission that can kill cells within a 2 mm radius [21]. By homogeneously spreading the virus throughout the tumor a more effective bystander effect is likely. Our confocal microscopy results showed that although the virus was distributed over the entire tumor, not all cells were infected with Ad5PB_RSV-NIS. However homogeneous viral distribution will result in overlapping “killing zones” resulting in larger areas of destruction of the tumor mass.

A second consequence of a better viral dispersion and NIS expression is an increase in the $t_{1/2}$ of radionuclide efflux. The $t_{1/2}$ parameters are dependent on the values of clearance and volume of distribution [22] and increased $t_{1/2}$ translates into a better retention time of the radioisotope within the tumor. Because the functional parameters of NIS are not likely dependent upon the concentration of the protein achieved by expression, we did not expect the tracer efflux $t_{1/2}$ to vary so widely between doses. The likely explanation for this variation in $t_{1/2}$ values is that the radionuclide is more readily re-up taken by neighboring cells after efflux when NIS expression is more robust at 1.88×10^7 genome copies/mg of tumor. The area under the curve between the two doses also indicates that the amount of radioisotope retained was 3 times higher in tumors receiving 10^{11} vp compared to those receiving 10^{10} vp, explaining the large difference in therapeutic outcome between the two doses. This phenomenon was previously implied from the decrease in the slopes of efflux curves as the number of cells expressing NIS increased [23]. Our results demonstrate this same effect *in vivo*. At 10^{11} vp more cells are infected and the expression is more diffuse, thus more overall cells express NIS, than at 10^{10} vp. The slopes of the efflux curves are 0.101 and 0.175 respectively at these two doses. Thus, our results agree with those of Dingli *et al*. while at the same time give a biological and therapeutic importance to the previously observed pharmacokinetic parameters. Higher NIS expression results in slower efflux of radionuclide from the tumor.

One of the major problems that needs to be circumvented for effective cancer gene therapy to be translated into the clinical setting is the limited ability to efficiently transduce tumors with effective levels of therapeutic transgenes [2425]. The data presented here corroborate this issue. But our findings also address a recent report from a clinical trials of a NIS expressing adenovirus that produced poor results with respect to uptake of radioiodine [26]. Barton et al. observed that the mean absorbed dose from administration of their vector into recurrent prostate cancers was well below the dose needed for a favorable therapeutic outcome. On the basis of our current results, it can be argued that to be successful, a NIS expressing virus needs to be efficiently spread within the tumor and NIS robustly expressed in order to reach the upper threshold and achieve more effective uptake.

A major limitation to viral spread is the high interstitial fluid pressure in solid tumors [27]. This limitation may be overcome by improving either the method of viral infusion or improving the replicating capabilities of the virus [28] or both. Until better methods of virus

delivery are developed, virus replicating capabilities and/or virus targeting will be the limiting factor(s) to viral spread [29, 30]. Thus, a rational approach should be undertaken in the design of viral vectors to improve these factors. In addition, for viruses destined to treat metastatic disease, modifications that alter liver tropism must also be an important consideration. For example, adenoviruses that contain modifications of important genes involved in replication, such as Ad-ONYX-015 [31, 32], should be avoided in favor of transcriptional dependent regulation because modifications of replication controlling genes can result in significant virus attenuation that seem unlikely to meet clinical needs [33]. In addition, viral genes, such as the E3 adenoviral death protein (ADP) gene, that play a role in adenoviral dispersal may be retained where possible to enhance viral spread [34]. Placing the NIS gene under the control of a potent promoter, as in our current construct, also results in stronger NIS expression. Finally, research on novel adenovirus serotypes and/or shielded viral capsid is also important as is that of serotypes that either de-targets the virus from liver sequestration and/or have low seroprevalance thus reducing the effects of pre-existing immunity [35–37].

In conclusion we present data that corroborates the efficacy of radiovirotherapy of non-thyroid malignancies. Our results however point out to the need for well-designed vectors capable of efficiently spreading within the tumor and resulting in robust NIS expression.

Materials and Methods

CRAd Construction

The structure Ad5PB_RSV-NIS CRAd was described elsewhere [9].

Cell Culture

The Androgen-dependent (LNCaP), prostate cancer cell line was cultured as described [38].

Animal Experiments

Experimental protocols were approved by the Mayo Foundation Institutional Animal Care and Use Committee. All animals were purchased from Harland Laboratories (Indianapolis, IN) and maintained in the Mayo Foundation animal barrier facilities.

Subcutaneous Tumor Model

Xenografts derived from the LNCaP cell line were established into the right flanks of 4–6-week-old athymic nude Foxn1nu mice (Harlan) by subcutaneous injection of 4×10^6 cells resuspended in 0.125 μl media and 0.125 μl of BD Matrigel basement membrane matrix (BD Biosciences, Bedford, MA). Mice were maintained on a low iodine diet and T4 supplementation (5mg/l) in their drinking water throughout the duration of the experimentation to maximize radioisotope uptake in the tumor and reduce uptake by the thyroid. The mice were examined daily for tumor development.

Viral injection

The virus was diluted in saline to the appropriate vp concentration. The volume of injection was 100 μl. Aliquots of the viral solution was deposit in three tumor regions. No pressure was applied for the injection other than normal thumb pressure

Titration of intratumoral virus by QPCR

LNCaP xenografts were established as described above. When tumors reached approximately 200 mm^3 they were injected with Ad5PB_RSV-NIS at 10^7, 10^9, or 10^{11} vp. Three days post-infection, mice were sacrificed and the tumors harvested. Three tumor samples weighing 30 mg each were taken from each tumor in each injection group and DNA was extracted using the DNEasy tissue kit (Qiagen, Valencia, CA, USA) with overnight lysis of tumor tissue in ATL buffer/Proteinase K. Each sample was assayed for Ad5PB_RSV-NIS genome copies using the Applied Biosystems TaqMan Universal PCR System according to the manufacturer's protocol (Applied Biosystems, Foster City, CA, USA). Briefly, reactions contained 300 nM of a forward primer GACGGCTACGACTGAATG from nt27837 to nt27854 in the Ad5 genome, 300 nM of a reverse primer complementing RSV sequences 118 bp upstream of the RSV promoter, CCGCTTTTCGCCTAAACACAC, and 250 nM of a TaqMan probe binding to the forward strand of the junction between Ad5 E3 sequences and the RSV sequences, 6′ FAM – ATATCTGGCCCGTACATCGCAGAT – Iowa Black FQ, (Integrated DNA Technologies, Coralville, IA, USA). Five μl of template DNA was amplified in 25 μl reactions using ABI Prism 7900HT Real Time PCR System (Applied Biosystems, Foster City, CA, USA). Genome copies per milligram of tissue were quantitated using a standard curve generated by amplification of known quantities of viral genomes.

Confocal microscopy

A total of four mice were subcutaneously engrafted with LNCaP as described previously. Mice received a single intratumoral dose of Ad5PB_RSV-NIS at 10^{11} vp. At day 3 and 10 two mice were sacrificed and the tumors removed. Control mice were injected with saline. All tumors were immersed in OCT compound, frozen, and sectioned to 4μm.

Mounted sections were selected from randomly selected locations spanning the whole tumor. Immunofluorescence staining was performed as previously described with some modifications [39]. Briefly, sections were fixed in 3% formalin and permeabilized with a 0.5% Saponin solution (PBS, 50 mg/ml normal mouse serum, and 0.5% Saponin) for 10 minutes on ice. Prior to hNIS antibody (mouse IgG 1:2000 dilution) treatment, slides were fixed and then blocked with 10% mouse serum. After wash with PBS, slides were re-blocked 10% donkey serum and NIS expression was revealed with a Texas red conjugated donkey Anti-mouse IgG (1:500) (Santa Cruz Biotechnology, Santa Cruz, CA). Sections were washed five times and blocked with 5% normal goat serum. Adenovirus hexon protein was stained with a goat polyclonal Adenovirus hexon protein conjugated with FITC (1:100) (Abcam Inc., Cambridge, MA). Sections were washed with PBS four times and 100μl of VECTASHIELD HardSet Mounting Medium with DAPI (Vector Laboratories, Burlingame, CA) was added as a counterstain and antifade agent. Texas red/FITC stained cells were analyzed on an LSM 510 confocal laser scanning microscope (Carl Zeiss, Inc., Thornwood, NY). Texas red was

excited with a 543 nm helium/neon laser. Emission for Texas red was selected with a 560–615 nm bandpass filter. FITC was excited at 488 nm using an argon laser. Emission for FITC was selected with a 505–550 nm band-pass filter. DAPI was excited at 364 nm using an argon laser. Emission for DAPI was captured through a 385–470 nm band-pass filter. Images were collected at 512 × 512 pixels resolution using a 40x C-apochromat water immersion lens (1.2 n.a.). Four stained sections from each of the time points listed above were analyzed by acquiring at least twenty-five images in each of the tumor slices. Adobe Photoshop CS5 digital imaging software (Adobe Systems Incorporated, San Jose, CA) was used to quantify the density of red pixels (hNIS) and green pixels (Adenovirus hexon protein) in each individual image as described [40].

Noninvasive imaging of xenografted tumors: Parallel hole and Pinhole

When engrafted LNCaP tumor size reached 200 mm^3, mice were randomly selected for each of four viral dosing groups (n=3) and given one intratumoral (IT) injection of Ad5PB_RSV-NIS CRAd at 10^7, 10^9, 10^{10} or 10^{11} vp respectively. Two mice were injected with saline as a control group. *In vivo* micro-SPECT-CT imaging was performed one hour after intraperitoneal injection of 0.5 mCi of ^{99}Tc. Animals were anesthetized using a Summit Medical Anesthesia Machine (Summit Medical Equipment Company, Bend, Oregon). Oxygen (2 LPM) was used throughout induction and exam. Induction was performed with 4% Isoflurane using an induction chamber. Mice were kept anesthetized throughout the full measurement by 2% Isoflurane using a nose cone. Images were acquired using a Gamma Medica XSPECT system (Gamma Medica, Inc., Northridge, CA). The SPECT scan was performed with a low energy, high resolution parallel-hole collimator and a single bore, low energy, 1 mm aperture pinhole collimator. For the parallel-hole scans a field of View of 12.5 cm, with a Reported Resolution of 1 to 2 mm was used. Sixty four projections, 10 sec/projection, were acquired with a total acquisition time of13:46 min. For pinhole imaging the radius of rotation was 5 cm giving a 6.84 cm field of view. Sixty four projections were acquired at 15 sec/projection using a 20% energy window with a Total Acquisition Time of 19:09 min. The CT Scan was performed with a continuous circular orbit of 256. Images were acquired at 80kVp and 0.28 mA with a Slice Thickness of 50μm and a Reported resolution of 43 μm. Images were analyzed using the PMOD Biomedical Image Quantification and Kinetic Modeling Software (PMOD Technologies, Switzerland). The level of ^{99}Tc uptake by the tumor was expressed as tumor activity in μCi/Tumor Volume (cc).

Efficacy Studies

Mice engrafted with LNCaP as above were divided in groups randomly (average group size n=10±3). The average tumor size at time 0 was 125±30 mm^3. One group of mice was used as control (C), a four groups of mice received a single intratumoral dose of Ad5PB_RSV-NIS at 10^7, 10^9, or 10^{11} vp (virotherapy V), the following four groups received a single intratumoral injection of Ad5PB_RSV-NIS at the indicated vp and 4 days later a single intraperitoneal dose of 3 mCi of ^{131}I. Tumor volume was measured twice weekly and mice were sacrificed as they met euthanization criteria established by Mayo Foundation Institutional Animal Care and Use Committee.

Radioisotope efflux studies

LNCaP xenograft bearing mice were divided into two groups randomly (average group size n=3). One group of mice received a single intratumoral dose of Ad5PB_RSV-NIS at 10^{10} vp; the second group received a dose of 10^{11} vp. Three days post infection a single intraperitoneal dose of 0.5 mCi of ^{99}Tc was administered. At time intervals mice were imaged and the images quantified as described above.

Statistics

All curve fittings were performed with SigmaPlot 10.0 (SigmaPlot Software). Survival was determined using Kaplan-Meier curves. The survival times were subjected to a Cox proportional hazards survival regression model.

Acknowledgments

This work was supported by Prostate SPORE grant P50 CA 091956, Donald J. Tindall, P.I., John C. Morris, Project Director.

The authors wish to thank Tracy Decklever at the Nuclear Medicine Animal Imaging Resource Mayo Clinic, Rochester for technical help and Dr. David Dingli at the Department of Molecular Medicine, Mayo Clinic, Rochester MN for helpful discussion.

References

1. Jemal A, Bray F, Center MM, Ferlay J, Ward E, Forman D. Global cancer statistics.[Erratum appears in CA Cancer J Clin, 2011 Mar–Apr;61(2):134]. CA Cancer J Clin. 2011; 61(2):69–90. [PubMed: 21296855]
2. Chiocca EA, Broaddus WC, Gillies GT, Visted T, Lamfers ML. Neurosurgical delivery of chemotherapeutics, targeted toxins, genetic and viral therapies in neuro-oncology. J Neurooncol. 2004; 69(1–3):101–17. [PubMed: 15527083]
3. McCormick F. Cancer gene therapy: fringe or cutting edge? Nat Rev Cancer. 2001; 1(2):130–41. [PubMed: 11905804]
4. Yamamoto M, Curiel DT. Cancer gene therapy. Technol Cancer Res Treat. 2005; 4(4):315–30. [PubMed: 16029053]
5. Carrasco N. Iodide transport in the thyroid gland. Biochim Biophys Acta. 1993; 1154(1):65–82. [PubMed: 8507647]
6. Jhiang SM, Cho JY, Ryu KY, DeYoung BR, Smanik PA, McGaughy VR, et al. An immunohistochemical study of Na+/I− symporter in human thyroid tissues and salivary gland tissues. Endocrinology. 1998; 139(10):4416–9. [PubMed: 9751526]
7. Van Nostrand D, Wartofsky L. Radioiodine in the treatment of thyroid cancer. Endocrinol Metab Clin North Am. 2007; 36(3):807–22. vii–viii. [PubMed: 17673129]
8. ELM. Carcinoma of follicular epithelium: Radioiodine and other treatments and outcomes. In: Braverman, LE.; Utiger, RD., editors. The Thyroid: A Fundamental and Clinical Text. 7. Lippincott - Raven; Philadelphia: 1996. p. 922-945.
9. Trujillo MA, Oneal MJ, McDonough S, Qin R, Morris JC. A probasin promoter, conditionally replicating adenovirus that expresses the sodium iodide symporter (NIS) for radiovirotherapy of prostate cancer. Gene Therapy. 2010; 17(11):1325–1332. [PubMed: 20428214]
10. Scholz IV, Cengic N, Baker CH, Harrington KJ, Maletz K, Bergert ER, et al. Radioiodine therapy of colon cancer following tissue-specific sodium iodide symporter gene transfer. Gene Ther. 2005; 12(3):272–80. [PubMed: 15510175]
11. Trujillo M, Oneal M, Davydova J, Bergert E, Yamamoto M, Morris J. Construction of an MUC-1 promoter driven, conditionally replicating adenovirus that expresses the sodium iodide symporter for gene therapy of breast cancer. Breast Cancer Research. 2009; 11(4):R53. [PubMed: 19635153]

12. Dwyer RM, Schatz SM, Bergert ER, Myers RM, Harvey ME, Classic KL, et al. A preclinical large animal model of adenovirus-mediated expression of the sodium-iodide symporter for radioiodide imaging and therapy of locally recurrent prostate cancer. Mol Ther. 2005; 12(5):835–41. [PubMed: 16054438]
13. Morris, JC. 2009. http://clinicaltrials.gov/ct/show/NCT00788307
14. Carlson SK, Classic KL, Hadac EM, Dingli D, Bender CE, Kemp BJ, et al. Quantitative molecular imaging of viral therapy for pancreatic cancer using an engineered measles virus expressing the sodium-iodide symporter reporter gene. AJR Am J Roentgenol. 2009American Journal of Roentgenology. 192(1):279–87.
15. Carlson SK, Classic KL, Hadac EM, Bender CE, Kemp BJ, Lowe VJ, et al. In vivo quantitation of intratumoral radioisotope uptake using micro-single photon emission computed tomography/computed tomography. Mol Imaging Biol. 2006; 8(6):324–32. 9(2):78–82. [PubMed: 17053863]
16. Groot-Wassink T, Aboagye EO, Glaser M, Lemoine NR, Vassaux G. Adenovirus biodistribution and noninvasive imaging of gene expression in vivo by positron emission tomography using human sodium/iodide symporter as reporter gene. Hum Gene Ther. 2002; 13(14):1723–35. [PubMed: 12396625]
17. Groot-Wassink T, Aboagye EO, Wang Y, Lemoine NR, Reader AJ, Vassaux G. Quantitative imaging of Na/I symporter transgene expression using positron emission tomography in the living animal. Mol Ther. 2004; 9(3):436–42. 13(6):1185–91. [PubMed: 15006611]
18. Dingli D, Peng KW, Harvey ME, Greipp PR, O'Connor MK, Cattaneo R, et al. Image-guided radiovirotherapy for multiple myeloma using a recombinant measles virus expressing the thyroidal sodium iodide symporter. Blood. 2004; 103(5):1641–6. [PubMed: 14604966]
19. Perron B, Rodriguez AM, Leblanc G, Pourcher T. Cloning of the mouse sodium iodide symporter and its expression in the mammary gland and other tissues. J Endocrinol. 2001; 170(1):185–96. [PubMed: 11431151]
20. Penheiter AR, Griesmann GE, Federspiel MJ, Dingli D, Russell SJ, Carlson SK. Pinhole micro-SPECT/CT for noninvasive monitoring and quantitation of oncolytic virus dispersion and percent infection in solid tumors. Gene Ther. 2011 advance online publication.
21. Carlin S, Cunningham SH, Boyd M, McCluskey AG, Mairs RJ. Experimental targeted radioiodide therapy following transfection of the sodium iodide symporter gene: effect on clonogenicity in both two-and three-dimensional models. Cancer Gene Ther. 2000; 7(12):1529–36. [PubMed: 11228531]
22. Tozer TN. Concepts basic to pharmacokinetics. Pharmacol Ther. 1981; 12(1):109–31. [PubMed: 7255535]
23. Dingli D, Bergert ER, Bajzer Z, O'Connor MK, Russell SJ, Morris JC. Dynamic iodide trapping by tumor cells expressing the thyroidal sodium iodide symporter. Biochem Biophys Res Commun. 2004; 325(1):157–66. [PubMed: 15522214]
24. Herrmann F. Cancer gene therapy: principles, problems, and perspectives. J Mol Med. 1995; 73(4): 157–63. [PubMed: 7627636]
25. Waehler R, Russell SJ, Curiel DT. Engineering targeted viral vectors for gene therapy. Nat Rev Genet. 2007; 8(8):573–87. [PubMed: 17607305]
26. Barton KN, Stricker H, Elshaikh MA, Pegg J, Cheng J, Zhang Y, et al. Feasibility of Adenovirus-Mediated hNIS Gene Transfer and 131I Radioiodine Therapy as a Definitive Treatment for Localized Prostate Cancer. Mol Ther. 2011; 19(7):1353–59. 13(6):1185–91. [PubMed: 21587209]
27. Boucher Y, Jain RK. Microvascular pressure is the principal driving force for interstitial hypertension in solid tumors: implications for vascular collapse. Cancer Res. 1992; 52(18):5110–4. 62(6):1884–9. [PubMed: 1516068]
28. Wang Y, Yuan F. Delivery of viral vectors to tumor cells: extracellular transport, systemic distribution, and strategies for improvement. Ann Biomed Eng. 2006; 34 (1):114–27. [PubMed: 16520902]
29. Kruyt FAE, Curiel DT. Toward a new generation of conditionally replicating adenoviruses: pairing tumor selectivity with maximal oncolysis. Hum Gene Ther. 2002; 13(4):485–95. 15(11):1022–33. [PubMed: 11874627]

30. Yamamoto M, Curiel DT. Current issues and future directions of oncolytic adenoviruses. Mol Ther. 2010; 18(2):243–50. 13(6):1185–91. [PubMed: 19935777]
31. Freytag SO, Rogulski KR, Paielli DL, Gilbert JD, Kim JH. A novel three-pronged approach to kill cancer cells selectively: concomitant viral, double suicide gene, and radiotherapy. Hum Gene Ther. 1998; 9(9):1323–33. 15(11):1022–33. [PubMed: 9650617]
32. Barton KN, Tyson D, Stricker H, Lew YS, Heisey G, Koul S, et al. GENIS: gene expression of sodium iodide symporter for noninvasive imaging of gene therapy vectors and quantification of gene expression in vivo. Mol Ther. 2003; 8(3):508–18. 13(6):1185–91. [PubMed: 12946325]
33. Bazan-Peregrino M, Carlisle RC, Hernandez-Alcoceba R, Iggo R, Homicsko K, Fisher KD, et al. Comparison of molecular strategies for breast cancer virotherapy using oncolytic adenovirus. Hum Gene Ther. 2008; 19(9):873–86. 13(17):2085–110. [PubMed: 18710328]
34. Doronin K, Toth K, Kuppuswamy M, Krajcsi P, Tollefson AE, Wold WS. Overexpression of the ADP (E3-11. 6K) protein increases cell lysis and spread of adenovirus. Virology. 2003; 305(2): 378–87. [PubMed: 12573583]
35. Doronin K, Shashkova EV, May SM, Hofherr SE, Barry MA. Chemical modification with high molecular weight polyethylene glycol reduces transduction of hepatocytes and increases efficacy of intravenously delivered oncolytic adenovirus. Hum Gene Ther. 2009; 20(9):975–88. 15(11): 1022–33. [PubMed: 19469693]
36. Shashkova EV, May SM, Barry MA. Characterization of human adenovirus serotypes 5, 6, 11, and 35 as anticancer agents. Virology. 2009; 394(2):311–20. 305(2):378–87. [PubMed: 19765790]
37. Weaver EA, Barry MA. Effects of shielding adenoviral vectors with polyethylene glycol on vector-specific and vaccine-mediated immune responses. Hum Gene Ther. 2008; 19(12):1369–82. 15(11):1022–33. [PubMed: 18778197]
38. Spitzweg C, Dietz AB, O'Connor MK, Bergert ER, Tindall DJ, Young CY, et al. In vivo sodium iodide symporter gene therapy of prostate cancer. Gene Ther. 2001; 8(20):1524–31. 12(3):272–80. [PubMed: 11704812]
39. Trujillo MA, Jiang SW, Tarara JE, Eberhardt NL. Clustering of the B cell receptor is not required for the apoptotic response. DNA Cell Biol. 2003; 22(8):513–23. [PubMed: 14565868]
40. Khoo TK, Coenen MJ, Schiefer AR, Kumar S, Bahn RS. Evidence for enhanced Thy-1 (CD90) expression in orbital fibroblasts of patients with Graves' ophthalmopathy. Thyroid. 2008; 18(12): 1291–6. [PubMed: 18976167]

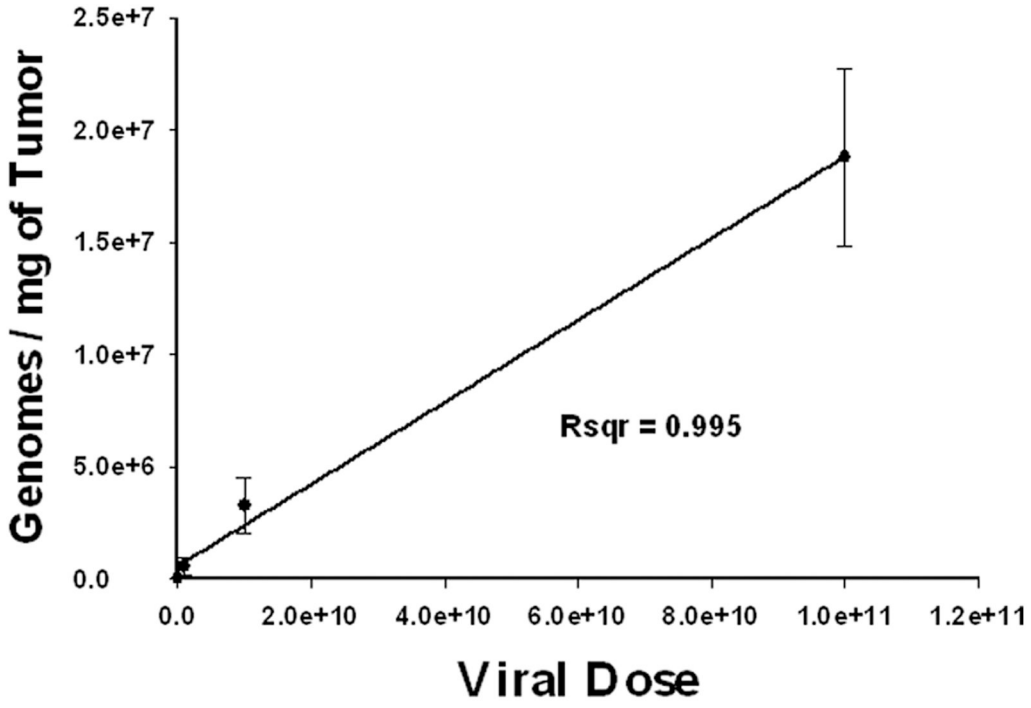

FIGURE 1. Correlation between injected and delivered viral dose after intratumoral injection

Mice were subcutaneously engrafted with LNCaP. When tumor reached approximately 200 mm^3 they were infected with Ad5PB_RSV-NIS at 10^7, 10^9, or 10^{11} vp. At day three post-infection, mice were sacrificed and the tumors harvested. Genome copies per milligram of tissue were quantitated by QPCR using a standard curve generated by amplification of known quantities of viral genomes.

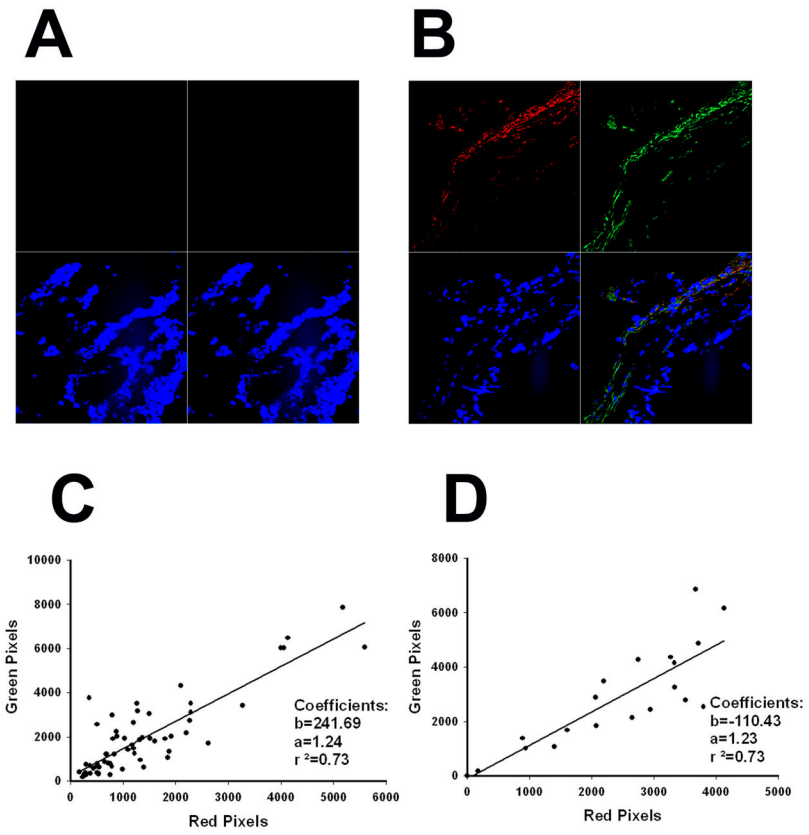

FIGURE 2. Correlation between viral presence and NIS expression

Mice were subcutaneously engrafted with LNCaP. When tumor reached approximately 200 mm^3 they were infected with Ad5PB_RSV-NIS at 10^{11} vp. At day three and ten post-infection mice were sacrificed and the tumors harvested and processed for confocal microscopy as described in Material and Methods.. A) Uninfected control. B) Ten days post-infection. Red quadrant hNIS, green quadrant Adenovirus hexon protein, blue quadrant DAPI, lower right quadrant merged image. The slides were quantified for red and green pixels using Adobe Photoshop CS5 digital imaging software (Adobe Systems Incorporated, San Jose, CA). C) Day three. D) Day ten.

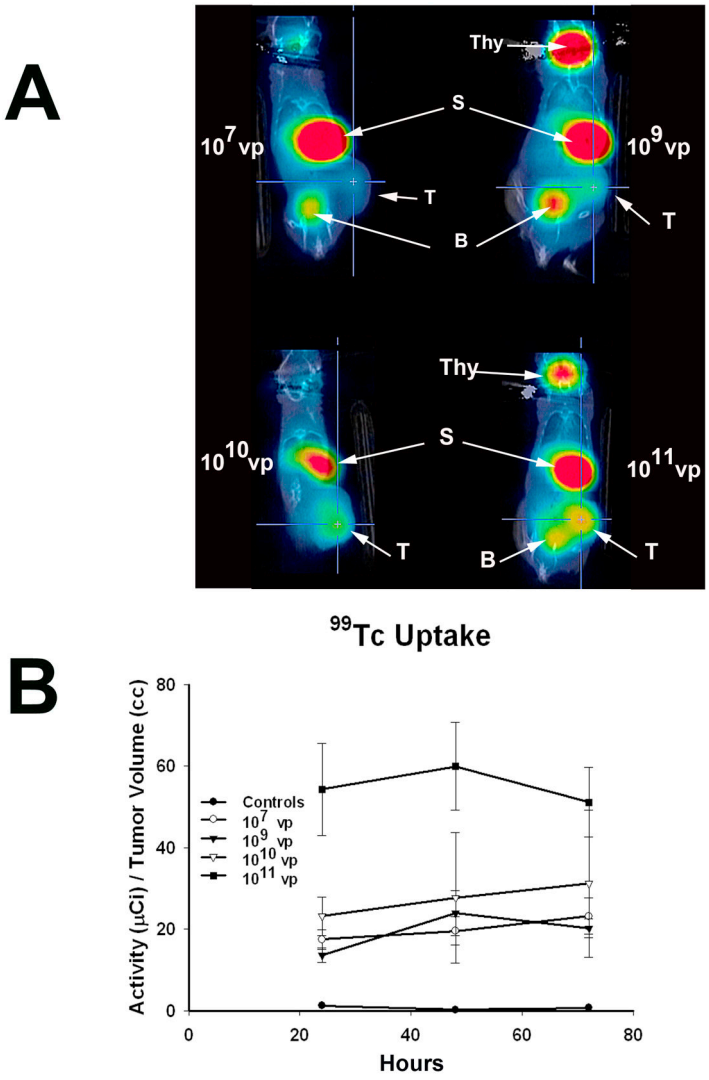

FIGURE 3. Radioiodine Imaging of Xenograft Tumors

A) LNCaP xenografted tumors were infected with Ad5PB_RSV-NIS at the indicated vp. Three days post-infection an injection of 0.5 mCi ^{99}Tc was given IP to all mice. Images were captured using a noninvasive micro SPECT-CT imaging system one hour after radioisotope administration. Thy: Thyroid, S: Stomach, B: Bladder, T: Tumor B) Kinetics of imaging was established by quantifying ^{99}Tc tumor uptake at the indicated times using the PMOD Biomedical Image Quantification and Kinetic Modeling Software (PMOD Technologies, Switzerland).

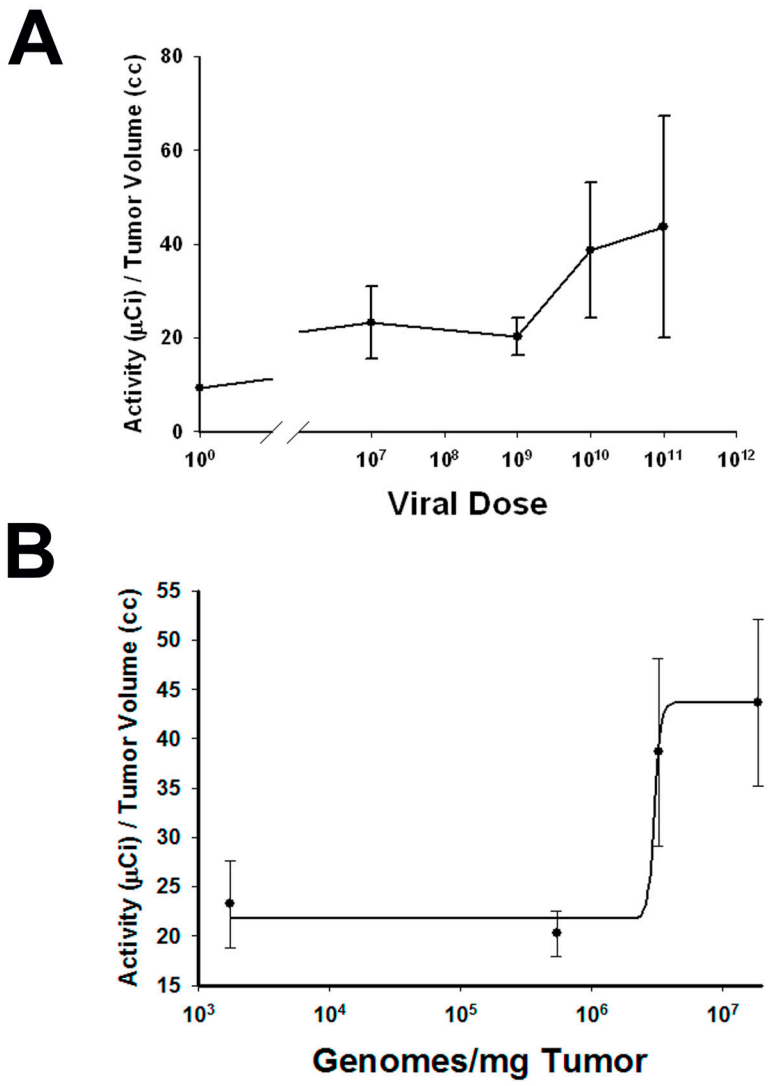

FIGURE 4. Viral dose response measured by in vivo NIS imaging

LNCaP tumors were established in the flanks of nude mice. When the xenografted tumors reached approximately 200 mm^3, a single dose of Ad5PB_RSV-NIS at 10^7, 10^9, 10^{10} and 10^{11} vp was administered intratumorally. NIS mediated ^{99}Tc uptake was visualized using non-invasive micro SPECT-CT imaging system. A) Quantification of ^{99}Tc tumor uptake at the indicated dose was done using the PMOD Biomedical Image Quantification and Kinetic Modeling Software (PMOD Technologies, Switzerland). B) Viral dose was transformed to viral genomes/mg of tumor using the equation fitting the curve depicted in figure 1. The resulting curve was fitted using a logistic model.

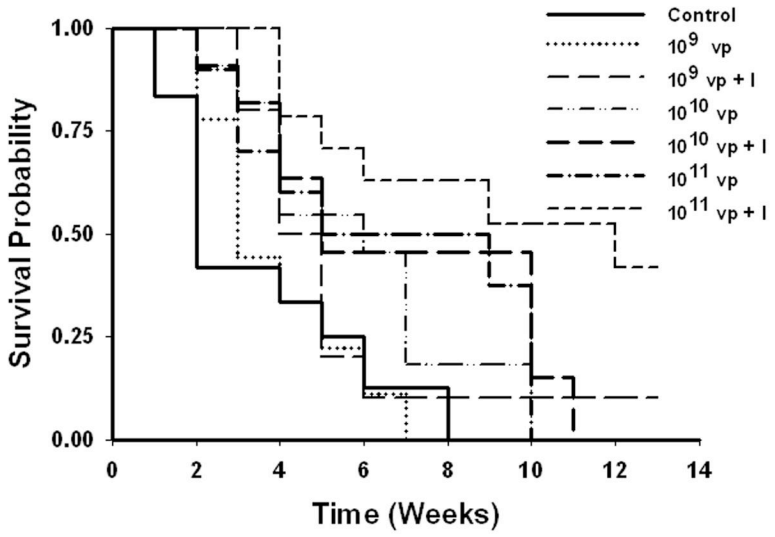

Cox proportional hazards survival regression

	Risk	Lo95%	Hi95%	p	pChi
Uninfected	-	-	-	-	0.0092
10^9	0.7640	0.3158	1.8483	0.5503	
10^9 +I	0.4306	0.1759	1.0542	0.0651	
10^{10}	0.4024	0.1720	0.9415	0.0358	
10^{10} +I	0.3695	0.1489	0.9168	0.0318	
10^{11}	0.3653	0.1470	0.9081	0.0302	
10^{11} +I	0.1519	0.0556	0.4148	0.0002	

FIGURE 5. Survival analysis

Mice engrafted with LNCaP were divided in groups randomly (average group size n=10±3). Time 0 is defined as the time of viral injection. The average tumor size at time 0 was 125±30 mm^3. At time 0, virus was injected intratumorally at the indicated vp. Four days post-injection a single intraperitoneal dose of 3 mCi of ^{131}I was administered (+I), Survival was plotted according to Kaplan-Meier and analyzed using the Cox proportional hazards survival regression.

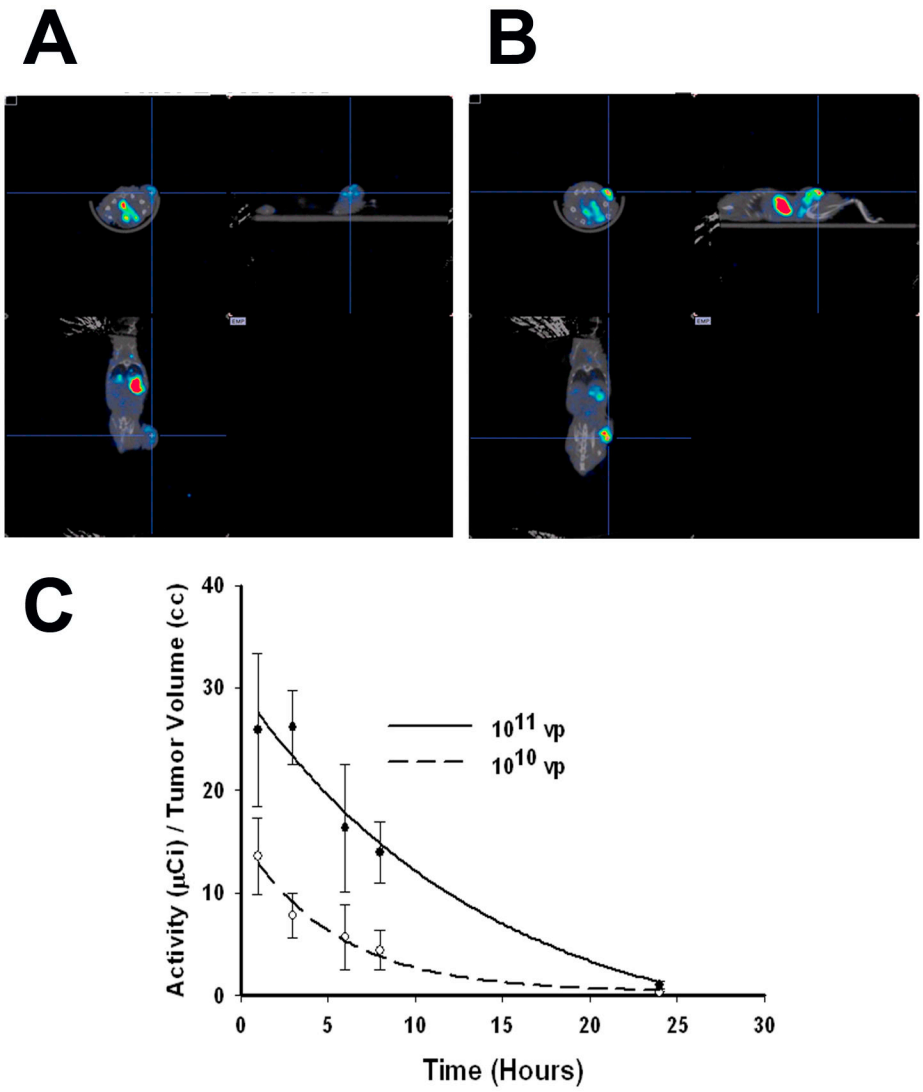

FIGURE 6. Pinhole imaging and radioisotope efflux

LNCaP xenografted tumors were infected with Ad5PB_RSV-NIS at 10^{10} or 10^{11} vp. Three days post-infection post-infection an injection of 0.5 mCi ^{99}Tc was given IP to all mice. Pinhole images were captured using a noninvasive micro SPECT-CT imaging system one hour after radioisotope administration. Images were quantified using the PMOD Biomedical Image Quantification and Kinetic Modeling Software (PMOD Technologies, Switzerland). A) Tumors injected with 10^{10} vp. B) Tumors injected with 10^{11} vp. C) Radioisotope efflux. Each point was done in triplicate.